

## Regeneration of NiAl<sub>2</sub>O<sub>4</sub> spinel type catalysts used in the reforming of raw bio-oil

Remiro, Aingeru; Arandia, Aitor; Oar-Arteta, Lide; Bilbao, Javier; Gayubo, Ana G.

**DOI**

[10.1016/j.apcatb.2018.06.005](https://doi.org/10.1016/j.apcatb.2018.06.005)

**Publication date**

2018

**Document Version**

Accepted author manuscript

**Published in**

Applied Catalysis B: Environmental

**Citation (APA)**

Remiro, A., Arandia, A., Oar-Arteta, L., Bilbao, J., & Gayubo, A. G. (2018). Regeneration of NiAl<sub>2</sub>O<sub>4</sub> spinel type catalysts used in the reforming of raw bio-oil. *Applied Catalysis B: Environmental*, 237, 353-364. <https://doi.org/10.1016/j.apcatb.2018.06.005>

**Important note**

To cite this publication, please use the final published version (if applicable). Please check the document version above.

**Copyright**

Other than for strictly personal use, it is not permitted to download, forward or distribute the text or part of it, without the consent of the author(s) and/or copyright holder(s), unless the work is under an open content license such as Creative Commons.

**Takedown policy**

Please contact us and provide details if you believe this document breaches copyrights. We will remove access to the work immediately and investigate your claim.

## Regeneration of NiAl<sub>2</sub>O<sub>4</sub> spinel type catalysts used in the reforming of raw bio-oil

Aingeru Remiro<sup>a,\*</sup>, Aitor Arandia<sup>a</sup>, Lide Oar-Arteta<sup>b</sup>, Javier Bilbao<sup>a</sup>, Ana G. Gayubo<sup>a</sup>

<sup>a</sup>Chemical Engineering Department, University of the Basque Country (UPV/EHU), P. O. Box 644, 48080. Bilbao, Spain. Phone: +34 946 015361. Fax: +34 946 013 500

<sup>b</sup>Catalysis Engineering / ChemE / TUDelft, Van der Maasweg 9, 2629 HZ Delft (The Netherlands)

\*email: aingeru.remiro@ehu.es

---

### Abstract

The regenerability of Ni catalysts in reforming reactions is a key factor for process viability. Accordingly, this study addresses the regeneration of two spinel NiAl<sub>2</sub>O<sub>4</sub> type catalysts by reaction-regeneration cycles in the oxidative steam reforming (OSR) of raw bio-oil. The spinel type catalysts were prepared by different methods including a supported Ni/La<sub>2</sub>O<sub>3</sub>- $\alpha$ -Al<sub>2</sub>O<sub>3</sub> catalyst and a bulk NiAl<sub>2</sub>O<sub>4</sub> catalyst. The experimental set-up consists of two units connected in series for i) the thermal treatment of bio-oil at 500 °C, in order to control the deposition of pyrolytic lignin, followed by; ii) the oxidative steam reforming (OSR) of the remaining oxygenates in a fluidized bed catalytic reactor. The conditions in the OSR reaction step were: 700 °C; oxygen/steam/carbon ratio (O/S/C), 0.34/6/1; space time, 0.75 g<sub>catalyst</sub>h/g<sub>bio-oil</sub> (for supported catalyst) and 0.15 g<sub>catalyst</sub>h/g<sub>bio-oil</sub> (for bulk catalyst). Three different strategies have been studied in the regeneration step by coke combustion, including the *in situ* regeneration inside the reactor at 650 °C and 850 °C, and the *ex situ* regeneration in an external oven at 850 °C, for 4 h in all the cases. The behavior of the fresh and regenerated catalysts has been explained according to their metallic properties, determined by different characterization techniques (temperature programmed reduction (TPR), X-ray diffraction (XRD), X-ray photoelectron spectroscopy (XPS), and transmission electronic microscopy (TEM)). According to these results, the combustion *ex situ* of the catalyst at 850 °C is able to completely regenerate the bulk catalyst, since these

regeneration conditions lead to the total recovery of the  $\text{NiAl}_2\text{O}_4$  spinel phase together with negligible loss of Ni on the surface in the catalyst. These novel results are crucial for future industrial implementation of the process.

*Keywords:* regeneration, Ni-Al spinel, reforming, bio-oil, hydrogen production

## 1. Introduction

Progress towards the Hydrogen Economy requires satisfying the increasing demand of H<sub>2</sub> both as clean fuel and as raw material for the petrochemical industry and agrochemistry. This needs to be done via the technological development of sustainable H<sub>2</sub> production routes from alternative sources to fossil fuels, thus reducing the negative environmental impact of current technologies [1-4]. In this scenario, biorefinery technologies have been proposed for converting different types of biomass into H<sub>2</sub> via different routes [5]. Among these routes, the steam reforming of bio-oil is an attractive option. Bio-oil may be produced at the place where the biomass is located (avoiding transportation), by fast pyrolysis of lignocellulosic biomass, at low temperature and with high yields and low environmental impact and using a simple reactor design [6,7]. The oxidative steam reforming (OSR) is an alternative of the steam reforming of bio-oil. Although the OSR gives lower H<sub>2</sub> yield than the steam reforming (SR), it requires less external energy supply, and with a proper oxygen/steam ratio in the feed, a thermoneutral regime can be achieved (autothermal reforming (ATR)) [8].

Major advances in the development of catalysts for the SR and the OSR have been made for Ni based catalysts, due to their high activity and selectivity to H<sub>2</sub>, besides their low cost [4,9]. Since the viability of the process is limited by catalyst deactivation, great attention has been paid to its causes. In this regard, coke deposition, sintering, phase transformation of Ni and poisoning by sulfur compounds have been all studied in the SR of both CH<sub>4</sub> and hydrocarbons [10-14]. Likewise, the same deactivation causes have been studied for the steam reforming of pure oxygenates, such as ethanol [15,16], glycerol [17,18], acetic acid [19] and ethanol-phenol mixtures [20]. Most of the studies on the deactivation of Ni catalysts in the SR of bio-oil focus on deactivation by coke. Coke deposition is the main cause of deactivation in the SR of bio-oil due to the ability of the oxygenates in bio-oil (mainly of phenolic compounds) to form deactivating coke, although sintering of Ni also contributes to some extent to the deactivation [21,22]. Likewise, Remiro et al. [23] proved that both coke deposition and sintering are the main causes for deactivation in the OSR of bio-oil.

Moreover, the regeneration of the catalysts has attracted great attention due to its importance for the economic viability of the reforming processes. In the SR of CH<sub>4</sub> and

hydrocarbons, the removal of coke is carried out by combustion or gasification [17,24-26], and the elimination of sulfur by steam treatment at high temperature (700-800 °C) [11-14]. Although coke or sulfur removal strategies have been widely studied, the real challenge is to achieve the reactivation of the catalyst subsequent to these regeneration treatments. In this regard, it should be mentioned that some authors have reported that the activity recovery is not complete due to Ni sintering [12].

The regenerability of the deactivated catalysts in the SR of model oxygenates and bio-oil has been scarcely studied in the literature, and besides, with contradictory results. Wu and Liu [27] studied the regeneration of a deactivated Ni/MgO-Al<sub>2</sub>O<sub>3</sub> catalyst in the SR of m-cresol. The total removal of the coke by combustion (600 °C) and gasification (850 °C) was effective for almost the complete (although not total) recovery of conversion and H<sub>2</sub> yield, with respect to the fresh catalyst, the activity of the catalyst regenerated by gasification being slightly higher. These authors attributed the activity loss to metal loss during the regeneration and metal sintering, evidenced by an increase in the average size of Ni crystallites.

Hereby, this work aims at studying the regenerability (by coke combustion with air) of two NiAl<sub>2</sub>O<sub>4</sub> spinel type catalysts which have been severely deactivated in the OSR of raw bio-oil. To this purpose, the effect of the coke combustion temperature and strategy (*in situ* in the reactor or *ex situ* in an external oven) on the recovery of the catalytic activity is analyzed, in order to determine the regeneration conditions needed to completely recover the activity of the fresh catalysts. The degree of activity recovery for both catalysts subsequent to regeneration is explained according to their metallic properties, which have been determined using different techniques: temperature programmed reduction (TPR), X-ray diffraction (XRD), X-ray photoelectron spectroscopy (XPS), and transmission electronic microscopy (TEM)).

The NiAl<sub>2</sub>O<sub>4</sub> spinel catalysts here studied include a bulk catalyst (prepared by co-precipitation, with 33 wt % of Ni) and a supported Ni/La<sub>2</sub>O<sub>3</sub>- $\alpha$ -Al<sub>2</sub>O<sub>3</sub> catalyst (prepared by impregnation, 10 wt % of Ni) calcined at high temperature in order to convert the Ni into the NiAl<sub>2</sub>O<sub>4</sub> spinel structure [28]. The bulk NiAl<sub>2</sub>O<sub>4</sub> catalyst was selected since it hinders to some extent the formation of coke and especially due to its high thermal stability, when used as catalyst for the steam reforming of CH<sub>4</sub> [29]. The selection of the supported Ni/La<sub>2</sub>O<sub>3</sub>- $\alpha$ -Al<sub>2</sub>O<sub>3</sub> catalyst was made considering its high activity, H<sub>2</sub>

selectivity and low coke formation in the SR of the aqueous fraction of bio-oil [21,30], raw bio-oil [31-33], ethanol [15,34], bio-oil/ethanol mixtures [28,35] and in the OSR of raw bio-oil [23]. The low coke deposition for this catalyst can be attributed to the presence of  $\text{La}_2\text{O}_3$  in the support, since this phase hinders the formation of coke and promotes its gasification [36]. The attenuating effect of  $\text{La}_2\text{O}_3$  on coke deposition may be attributed to: i) the capacity of  $\text{La}_2\text{O}_3$  for water adsorption [37,38] that helps to prevent the adsorption of coke precursors and so their growth mechanism (through oligomerization, aromatization and condensation reactions); ii) the ability to generate surface oxygen through the formation of lanthanum oxycarbonate ( $\text{La}_2\text{O}_2\text{CO}_3$ ) which is active to react with coke and clean the Ni surface [38-41].

## 2. Experimental

### 2.1. Catalysts

The  $\text{Ni}/\text{La}_2\text{O}_3\text{-}\alpha\text{Al}_2\text{O}_3$  catalyst (denoted as supported catalyst) was prepared with 10 wt % Ni and 9 wt % La using a method reported elsewhere [36]. The catalyst was calcined at 850 °C in order to boost the formation of  $\text{NiAl}_2\text{O}_4$  spinel, thus providing high thermal stability in the reforming reaction which takes place at high temperature. In a previous work (results not shown) it was observed that supported catalyst calcined at 550 °C (corresponding to the maximum activity) had notably lower catalytic activity after its regeneration by coke combustion.

The bulk  $\text{NiAl}_2\text{O}_4$  catalyst (denoted as bulk catalyst) was synthesized by the coprecipitation method [42,43] using aqueous solutions of hexahydrated nickel nitrate ( $\text{Ni}(\text{NO}_3)_2 \cdot 6\text{H}_2\text{O}$ , Panreac, 99 %) and nona-hydrated alumina nitrate ( $\text{Al}(\text{NO}_3)_3 \cdot 9\text{H}_2\text{O}$ , Panreac, 98 %), and ammonium hydroxide as the precipitating agent ( $\text{NH}_4\text{OH}$  0.6 M, Fluka, 5 M). After filtration, the precipitate was washed with distilled water to remove the ammonium ions, then dried for 12 h and finally, calcined at 850 °C for 4 h. The amount of Ni and Al nitrate salt precursors were those corresponding to 33 wt % of Ni for the  $\text{NiAl}_2\text{O}_4$  spinel.

The fresh catalysts have been characterized by  $\text{N}_2$  adsorption-desorption in an *Autosorb iQ2* equipment from *Quantachrome*. For the fresh catalysts, the BET surface areas are  $37.6 \text{ m}^2\text{g}^{-1}$  and  $93.5 \text{ m}^2\text{g}^{-1}$  for the supported catalyst and the bulk catalyst, respectively, and the pore volumes are  $0.14 \text{ cm}^3\text{g}^{-1}$  and  $0.18 \text{ cm}^3\text{g}^{-1}$ .

The catalysts have been characterized according to different techniques (described below) at different stages of a reaction-regeneration cycle (Fig. 1).

### Figure 1

Temperature programmed reduction (TPR) measurements were carried out on an *AutoChem II 2920 Micromeritics* using a stream with 10 % volume of H<sub>2</sub> in He (50 cm<sup>3</sup>/min): the sample (approximately 150 mg) was firstly degassed at 200 °C and subsequently heated in a reducing stream from 50 to 900 °C following a 5 °C/min heating ramp. An isopropanol trap was used to remove water generated during reduction. A thermal conductivity detector (TCD) was used to monitor hydrogen consumption.

The X-ray diffraction (XRD) analyses were measured on a *Bruker D8 Advance* diffractometer with a CuK<sub>α1</sub> radiation, in order to calculate the average Ni particle size by using the Scherrer equation. The device is equipped with a Germanium primary monochromator, *Bragg-Brentano* geometry and with a CuK<sub>α1</sub> wavelength of 1.5406 Å, corresponding to an X-ray tube with Cu anticathode. *Sol-X* dispersive energy detector was employed, with a window optimized for CuK<sub>α1</sub> for limiting the fluorescence radiation. Data collection was carried continuously, from 10° to 80° with step of 0.04° in 2θ and measurement time per step of 300 s.

The oxidation state of the metal on the catalyst surface has been determined by X-ray photoelectron spectroscopy (XPS), in a SPECS system equipped with a Phoibos 150 1D-DLD analyzer and Al K<sub>α</sub> monochromatic radiation (hν, 1486.6 eV). The binding energy of C1s peak was set at 284.6 eV to correct the material charging and the spectrometer was previously calibrated with Ag 3d 5/2 peak (368.28 eV).

The Ni particle size distribution (PSD) was determined from transmission electron microscopy (TEM) images (a *Philips SuperTwin CM200*). Up to 300 individual metal particles were counted for each catalyst.

### 2.2. Bio-oil production and composition

The raw bio-oil was obtained by flash pyrolysis of pine sawdust at 480 °C, in a semi-industrial demonstration plant (Ikerlan-IK4 technology center, Alava, Spain), with a biomass feeding capacity of 25 kg/h [44]. The physical-chemical properties of the bio-

oil are as follows: water content, 37 wt %; density, 1.107 g ml<sup>-1</sup>; viscosity at 40 °C, 8.5 cP; pH, 3.3; empiric formula obtained by CHO analysis, C<sub>4.21</sub>H<sub>7.14</sub>O<sub>2.65</sub> (dry basis). The high heating value (HHV) is 21.66 MJ kg<sup>-1</sup> (determined by the equation proposed by Channiwala and Parikh [45]). The detailed raw bio-oil composition, determined by GC/MS analyser (Shimadzu QP2010S device) was reported previously [23]. The sulfur content in the bio-oil has been analyzed by elemental analysis (*LECO TruSpec CHN Macro* equipment, with 0.2 % detection threshold) as well as by gas chromatography (Agilent 7890 A equipment provided with a pulsed flame photometric detector (PFPD) for detection of sulfur containing compounds, with a detection threshold of 10 ppm). The adequacy of the latter equipment for measuring the sulfur content in highly desulfurized refinery streams has been proven in previous works [46]. A very low content of sulfur has been determined for the bio-oil used (31 ppm, below the detection threshold of the elemental analysis equipment), which is in agreement with previous results in literature [47,48].

### 2.3. Reaction equipment and operating conditions

The catalytic runs have been performed in an automated reaction equipment (*MicroActivity Reference* from *PID Eng&Tech*, Madrid, Spain) provided with two units in series (thermal step and catalytic step) of stainless steel [23]. The thermal step consists of a U-shaped tube at 500 °C for the controlled deposition of pyrolytic lignin (a solid residue formed by repolymerization of some oxygenates in bio-oil, mainly those derived from lignin pyrolysis). In this step, 11 wt % of the oxygenates in the raw bio-oil was deposited and the corresponding molecular formula of the bio-oil exiting this step is C<sub>3.8</sub>H<sub>7.7</sub>O<sub>2.9</sub> (water-free basis). The catalytic step consists in a fluidized bed reactor (with 22 m internal diameter) where the volatile stream exiting the thermal treatment is reformed. The use of this two-step system minimizes operating problems (such as plugging of reactor piping) as well as catalyst deactivation in the reforming step. This strategy for valorizing raw bio-oil, with separation of pyrolytic lignin by a thermal treatment prior to the *in-line* catalytic transformation of bio-oil, allows a higher fraction of bio-oil oxygenates to be valorized to H<sub>2</sub> compared to other strategies such as water addition to separate bio-oil into two phases (aqueous and organic) followed by the aqueous bio-oil reforming (given that a noticeable amount of oxygenates is removed from the raw bio-oil in the organic phase by the water addition) [49].



In the fluidized bed reactor, the catalyst (with particle size of 150-250  $\mu\text{m}$  to avoid internal diffusional limitations) is mixed with inert solid (SiC, with 37  $\mu\text{m}$  particle size) (inert/catalyst mass ratio  $> 8/1$ ) in order to assure a correct fluidization regime. The different particle size of both solids (inert and catalyst) facilitates their separation after the reaction by sieving, which is necessary for the characterization of the *in-situ* regenerated catalyst and for the *ex-situ* regeneration of the catalyst without the inert solid. It should be noticed that  $\text{O}_2$  is fed at the entrance of the reforming reactor in order to prevent the oxidation of the feed in the first step (thermal treatment), thus maximizing the  $\text{H}_2$  yield in the two step reaction system [50].

Prior to the reaction, the catalyst is reduced *in situ* with  $\text{H}_2\text{-N}_2$  stream (10 vol % of  $\text{H}_2$ ) for 4 h at 850  $^\circ\text{C}$ , which is the maximum temperature attainable in the reactor and it is necessary to ensure the reduction of most of the oxidized Ni species according to TPR results shown in Figs. 3 and 8 (sections 3.1.2 and 3.2.2, respectively). Subsequent to reduction,  $\text{Ni}^0/\text{La}_2\text{O}_3\text{-Al}_2\text{O}_3$  or  $\text{Ni}^0/\text{Al}_2\text{O}_3$  are formed for supported or bulk catalysts, respectively.

The products stream is analyzed in-line with a *MicroGC 490* from *Agilent*, equipped with four analytic channels: molecular sieve MS5 for quantifying  $\text{H}_2$ ,  $\text{N}_2$ ,  $\text{O}_2$ ,  $\text{CH}_4$  and  $\text{CO}$ ; Plot Q for  $\text{CO}_2$ ,  $\text{H}_2\text{O}$  and  $\text{C}_2\text{-C}_4$  hydrocarbons; CPSIL for  $\text{C}_5\text{-C}_{11}$  hydrocarbons, and; Stabilwax for oxygenated compounds.

In order to analyze the recovery of activity subsequent to catalyst regeneration, a reaction-regeneration cycle has been carried out, with fixed values of operating conditions in the reaction step and different conditions in the regeneration step. The conditions in the reaction steps have been as follows: 700  $^\circ\text{C}$ ; atmospheric pressure; steam/carbon (S/C) molar ratio in the feed, 6, which is obtained by co-feeding water (307 *Gilson pump*) with the raw bio-oil (*injection pump Harvard Apparatus 22*); oxygen/carbon ratio (O/C), 0.34; space time, 0.75  $\text{g}_{\text{catalyst}}\text{h}/\text{g}_{\text{bio-oil}}$  for supported catalyst, and 0.15  $\text{g}_{\text{catalyst}}\text{h}/\text{g}_{\text{bio-oil}}$  for bulk catalyst (a lower value, due to its higher activity).

The regeneration steps consisted in the coke combustion with air following two strategies: i) *in situ*, inside the reactor and mixed with the inert SiC (at 650 and 850  $^\circ\text{C}$ ), in fluidized bed regime and 100  $\text{cm}^3/\text{min}$  of air, and; ii) *ex situ*, in an oven at 850  $^\circ\text{C}$  in air atmosphere. In this second case, the catalyst is regenerated alone, after the separation

of the SiC inert used for the reaction. The lower temperature for coke combustion (650 °C) was determined based on the Temperature Programmed Oxidation (TPO) analysis of the deactivated catalysts, which was carried out in a *TA Instrument SDT 2960* thermobalance coupled to a mass spectrometer *Thermostar Balzers Instrument* for monitoring the signal corresponding to the CO<sub>2</sub>. The variation of coke content during the combustion (DTG signal) has been quantified from the CO<sub>2</sub> spectroscopic signal, instead of the thermogravimetric signal, because Ni oxidation during the combustion masks the latter signal. According to the TPO results of both deactivated catalysts (Fig. S1 in the supporting information), the combustion at 650 °C or higher temperature assures that total removal of coke. Moreover, the removal of coke in the different regeneration conditions has been checked by chromatographic analysis of the CO<sub>2</sub> signal in the *MicroGC 490* from *Agilent* during each regeneration step. It should be noted that even if some residual coke was still remaining after the regeneration treatment it would be very low (so that the CO<sub>2</sub> signal would be below the detection threshold of the MicroGC) and, moreover, it would correspond to a coke difficult to burn deposited on the support and, consequently, with low impact on the catalyst deactivation. The low impact on deactivation of the coke deposited on the support for Ni-based catalysts has been proven in previous works, since the main responsible of deactivation is the coke deposited on the metallic sites (encapsulating coke), which is burnt at low temperature, as its combustion is catalyzed by the metal [22,32,33,51,52].

#### 2.4. Reaction indices

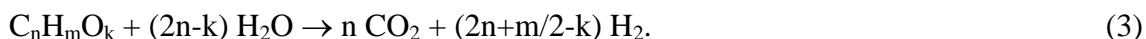
The following reaction indices have been used for quantifying the behavior of the catalysts:

$$\text{Bio-oil conversion: } X_{\text{bio-oil}} = \frac{F_{\text{in}} - F_{\text{out}}}{F_{\text{in}}} \quad (1)$$

where  $F_{\text{in}}$  and  $F_{\text{out}}$  are the molar flow rate of bio-oil at the reactor inlet and outlet, respectively, in C units contained.

$$\text{H}_2 \text{ yield: } Y_{\text{H}_2} = \frac{F_{\text{H}_2}}{F_{\text{H}_2}^0} 100 \quad (2)$$

where  $F_{H_2}$  is the  $H_2$  molar flow rate in the product stream and  $F_{H_2}^0$  is the stoichiometric molar flow rate (referred to the C units contained in the bio-oil fed into the reforming reactor), which has been evaluated as  $(2n+m/2-k)/n \cdot F_{in}$ , according to the global stoichiometry for bio-oil steam reforming (SR) (including the water gas shift (WGS) reaction):



The yield of carbon-containing products ( $CO_2$ ,  $CO$ ,  $CH_4$  and light hydrocarbons):

$$Y_i = \frac{F_i}{F_{in}} 100 \quad (4)$$

where  $F_i$  is the molar flow rate of each compound, in C units contained.

$CH_4$  and light hydrocarbons (mainly ethylene) are formed by thermal routes (decomposition/cracking reactions of oxygenates) and their relative importance in the OSR decreases under conditions that favor the progress of the catalyzed reactions (reforming and WGS), such as high space time [53,54].

The flow rates in Eqs. (1), (2) and (4) have been determined by C balances with the inlet stream being the bio-oil at the thermal unit inlet (0.08 ml/min) and the outlet stream the reaction products (quantified by gas chromatography) and taking into account the amount of pyrolytic lignin deposited in the thermal unit. Accordingly, a balance closure above 95 wt % is attained, with the relative error (based on replicates) being lower than 4 %.

### 3. Results

#### 3.1. On the regenerability of the supported catalyst

##### 3.1.1. Performance in reaction and regeneration steps

Fig. 2 shows the evolution with time on stream of the reaction indices (bio-oil conversion and yield of different products) for the fresh catalyst and after its regeneration according to each of the three strategies described in section 2.3. The fresh catalyst (black dots) at zero time on stream (TOS) reaches full conversion and the yield of  $H_2$ ,  $CO_2$  and  $CO$  are 78 %, 90 % and 10 %, respectively, with negligible formation of  $CH_4$  and light hydrocarbons. These reaction indices are stable for approximately 1 h TOS and subsequently a breakthrough curve is observed, with rapid variation of the

reaction indices. As a result, the bio-oil conversion and the H<sub>2</sub> and CO<sub>2</sub> yields drop to 85 %, 20 % and 27 %, respectively, after 150 min TOS, due to catalyst deactivation for the reforming reactions (of oxygenates and carbon byproducts (CH<sub>4</sub> and light hydrocarbons)), and the water gas shift (WGS) reaction. Consequently, the yields of CO, CH<sub>4</sub> and hydrocarbons increase (up to 36 %, 8 % and 14 %, respectively). After 150 min TOS, the reaction indices evolve very slowly, approaching values corresponding to those of thermal routes (i.e., without catalyst) [32,53].

### Figure 2

The activity recovery is not complete for neither of the *in situ* regenerated catalysts at 650 °C and 850 °C (green dots and blue dots in Fig. 2, respectively) although the activity is higher for the catalyst treated at 850 °C. Moreover, the deactivation of the partially regenerated catalyst is faster than that of the fresh catalyst. Otherwise, the *ex situ* regeneration of the catalyst in an external oven at 850 °C is able to almost completely recover the activity of the fresh catalyst. In this case, full conversion of bio-oil is reached at zero TOS and the product yields are almost the same to those obtained with the fresh catalyst. Nevertheless, the stability of the regenerated catalyst is slightly lower than that of the fresh catalyst, so that the decrease in bio-oil conversion and H<sub>2</sub> and CO<sub>2</sub> yields begins at slightly lower value of TOS for this regenerated catalyst.

In order to quantify the activity recovery after each regeneration treatment, the regeneration efficiency is defined in Eq. (5) and calculated by comparing the accumulated production of H<sub>2</sub> for the regenerated and the fresh catalyst:

$$\eta_{regeneration} = \frac{\left[ \int_0^{t_f} F_{H_2} dt \right]_{regenerated} - (F_{H_2}^* \cdot t_f)_{regenerated}}{\left[ \int_0^{t_f} F_{H_2} dt \right]_{fresh} - (F_{H_2}^* \cdot t_f)_{fresh}} \cdot 100$$

$$= \frac{\left[ \int_0^{t_f} Y_{H_2} dt \right]_{regenerated} - (Y_{H_2}^* \cdot t_f)_{regenerated}}{\left[ \int_0^{t_f} Y_{H_2} dt \right]_{fresh} - (Y_{H_2}^* \cdot t_f)_{fresh}} \cdot 100 \quad (5)$$

where  $Y_{H_2}^*$  is the residual H<sub>2</sub> yield (formed through thermal routes when the catalyst is totally deactivated), and  $t_f$  is the duration of the reaction.

In this manner, the efficiency for the catalysts regenerated *in situ* is 2 % and 35 % at 650 °C and 850 °C, respectively and 85 % for the catalyst regenerated *ex situ* at 850 °C.

It should be noted that, as mentioned in section 2.3, all the conditions used for the regeneration assure the complete removal of coke. Consequently, the aforementioned results prove that coke deposition is not the only deactivation cause of the catalyst in the OSR at 700 °C, since its complete removal is not enough for the total recovery of the catalytic activity. Furthermore, sulfur poisoning was discarded as possible responsible of the activity loss observed in the regenerated catalysts since: i) on the one hand, there is a very low sulfur content in the raw bio-oil used in this work (as indicated in section 2.2); ii) on the other hand, it has been proven (Figure S2 in supported information) that there is not a further recovery of the reaction indices for the catalyst regenerated *in situ* at 650 °C once it has been subjected to an additional steam treatment at 800 °C (which has been proven in literature to be efficient for sulfur removal on deactivated catalysts [11-14]). Consequently, in case the low content of sulfur in the bio-oil contributed to any extent to catalyst deactivation by poisoning of the metal sites in the reaction step (black dots in Figure 2), the sulfur deposited would be completely removed together with the coke during the *in-situ* combustion at 650 °C. Accordingly, the activity loss for the regenerated catalysts should be due to a change in the metallic properties during the reaction and regeneration steps. In fact, both the reaction and the regeneration conditions noticeably affect these metallic properties, as shown in the following section.

### 3.1.2. Metallic properties of the catalyst

The physical-chemical properties and microscopic morphology of the fresh, deactivated and regenerated catalysts have been analyzed with several techniques (TPR, XRD, XPS and TEM). These properties have been related to the kinetic behavior of the fresh and regenerated catalysts in order to ascertain the causes of the catalytic activity loss and recovery.

Fig. 3 shows the TPR profiles for the fresh and the regenerated catalysts. No reduction peaks are present for the deactivated catalyst (results not shown), thus meaning that oxidation of Ni is not one of the causes for the catalytic activity loss. The fresh catalyst shows a main peak with its maximum at 770 °C, which corresponds to the reduction of the NiAl<sub>2</sub>O<sub>4</sub> spinel phase. Two other (very small) reduction peaks appear in the 300-450

°C range, corresponding to the reduction of NiO species having different interaction strength with the support, and therefore different reducibility [15,28,55,56]. The catalysts regenerated *in situ* at 650 and 850 °C in the fluidized bed show the peaks corresponding to both NiAl<sub>2</sub>O<sub>4</sub> and NiO species in the TPR profile. The existence of several reduction peaks in the 250-550 °C range evidences the different NiO species present in this sample. Reduction peaks below 380 °C correspond to the reduction of bulk NiO clusters with low interaction with the support and the peaks between 400 and 700 °C are ascribed to the reduction of dispersed NiO<sub>x</sub> species interacting more strongly with the support [15]. The increase in the reduction peak for the NiAl<sub>2</sub>O<sub>4</sub> spinel when increasing the *in situ* regeneration temperature from 650 to 850 °C is possibly due to the higher reassembly rate of NiO and Al<sub>2</sub>O<sub>3</sub> to form the spinel. The increase in the NiAl<sub>2</sub>O<sub>4</sub> spinel/NiO ratio when the calcination temperature was increased has already been established in a previous study about the catalyst preparation [28]. The catalyst regenerated *ex situ*, in the oven at 850 °C, has a similar TPR profile to that of the fresh catalyst, where the NiAl<sub>2</sub>O<sub>4</sub> spinel phase is prevailing (reduction maximum at 770 °C).

### Figure 3

Fig. 4 shows the XRD diffractograms corresponding to the fresh and the regenerated catalysts, before (Fig. 4a) and after reduction at 850 °C for 4 h (Fig. 4b). Fig. 4b also includes the diffractogram of the deactivated catalyst. Fig. 4a evidences that NiAl<sub>2</sub>O<sub>4</sub> spinel (at  $2\theta = 19.2, 31.3, 36.9, 44.6, 59.7$  and  $66.7^\circ$ ) is the main Ni specie in both the fresh oxidized catalyst and the catalyst regenerated *ex situ* at 850 °C. Meanwhile, for the catalysts regenerated *in situ* in the fluidized bed, the presence of NiO (at  $2\theta = 37.4$  and  $62.9^\circ$ ) is more noticeable and becomes more significant at lower regeneration temperature. These results are in agreement with TPR results (Fig. 3). The joint analysis of TPR and XRD results in Figs. 3 and 4, respectively, together with the performance of the catalysts (Fig. 2) points to the presence of NiAl<sub>2</sub>O<sub>4</sub> species as the responsible of the higher activity of the fresh catalyst compared to the *in-situ* regenerated catalysts.

### Figure 4

The presence of Ni<sup>0</sup> is observed in the XRD diffractograms for all the reduced catalysts (peaks at  $2\theta = 44.7^\circ$  and  $51.8^\circ$  in Fig. 4b) regardless the initial composition (NiO or NiAl<sub>2</sub>O<sub>4</sub> species), and some NiAl<sub>2</sub>O<sub>4</sub> species still remain in all the reduced samples due

to the high temperature needed for their total reduction (as observed in Fig. 3). Nevertheless, a significant difference is observed in the width of the Ni<sup>0</sup> peaks for the catalyst after the different regeneration treatments. This difference highlights the important role the deactivation and the regeneration conditions play on the Ni dispersion on the catalyst. Table 1 shows the average Ni<sup>0</sup> crystallite sizes calculated according to the Scherrer equation from the XRD diffractograms.

**Table 1**

The deactivated catalyst has bigger average Ni<sup>0</sup> crystallite size (29 nm) than the fresh catalyst (21 nm), which evidences metal sintering along the reforming reaction at 700 °C. The decrease in the metal particle size after regeneration of the catalyst by coke combustion at high temperature suggests metal redispersion. When the regeneration is carried out *ex situ* at 850 °C in air atmosphere (without gas flow), the average crystallite size reaches 16 nm, which is even lower than that of the fresh catalyst (21 nm). These results in Table 1 (obtained by XRD) have been confirmed by TEM analysis (Fig. 5). The metallic Ni<sup>0</sup> particle size distribution (PSD) has been determined by means of the TEM images for the catalyst in different states (fresh, deactivated and regenerated) (Fig. 6). For the deactivated catalyst (Fig. 5b), TEM analysis evidences the formation of filamentous coke together with the presence of a Ni<sup>0</sup> particle at the end of the filament. This Ni particle detachment from the surface of the support due to the growth of carbon filaments has been also observed for Ni catalysts in other reactions [51,57-59]. The average Ni<sup>0</sup> particle size determined by TEM increases from 18.9 nm for the fresh catalyst to 30.5 nm for the deactivated catalyst, once again proving the sintering of Ni particles during the reaction. The lower average Ni<sup>0</sup> crystal size (16.6 nm) corresponds to the catalyst regenerated *ex situ* at 850 °C, which is even slightly lower than that of fresh catalyst. The catalyst regenerated *in situ* at 650 °C has 24.7 nm average Ni<sup>0</sup> crystal size and a wide PSD, with particles bigger than 30 nm.

**Figure 5**

**Figure 6**

The results shown in Table 1 and Figs. 5 and 6 confirm that besides coke deposition, sintering of Ni particles contributes to great extent to the catalyst deactivation in the studied conditions. Consequently, the regeneration conditions employed for coke

removal should involve metal redispersion in order to be effective for activity recovery. The regeneration by coke combustion at 650 °C, although is effective for completely removing the deposited coke in the reaction, is not enough for recovering the initial catalytic activity of the fresh catalyst, since the Ni particle size remains big (and consequently, the metal active surface is low). However, the regeneration at high temperature (850 °C) is able to redisperse the Ni metal particles, this phenomenon being more pronounced when the regeneration is carried out *ex situ* in the oven (air atmosphere without gas flow). In the latter case, the catalytic activity recovery is as high as 85 % in terms of regeneration efficiency (Eq. (5)). Although the regenerated catalyst recovers its spinel type structure, and the Ni redispersion (after reduction) is even better than that for the fresh catalyst, the regenerated catalyst is not able to recover its initial activity completely (that of the fresh catalyst). Thus, the decrease in the surface Ni particles after the reaction-regeneration cycle is likely to be the cause of this activity loss.

The decrease in surface Ni<sup>0</sup> has been studied by XRD and XPS analysis for the catalyst after the different treatments. The results in Table 1 have been calculated as the ratio between the area of the Ni<sup>0</sup> peak ( $2\theta = 44.7^\circ$ ) in Fig. 3b and the area of the LaAlO<sub>3</sub> peak ( $2\theta = 33.5^\circ$ ), which is more pronounced and has a similar size for the catalyst after the different treatments. This ratio allows a qualitative comparison of the amount of Ni<sup>0</sup> in the different catalyst states. According to these results, the loss of Ni<sup>0</sup> active centers is about 10-20 % after the reaction-regeneration cycle. Nevertheless, the experimental error does not allow determining the effect of the different regeneration strategies on the loss of active Ni<sup>0</sup> centers. XPS results in Table 2 show the surface mass content of the different elements in the catalyst (including C in the deactivated catalyst). According to this technique, the regenerated catalyst has 5.5 and 7 wt % surface Ni content, which is notably lower than the 17 wt % in the fresh catalyst. A possible cause for the decrease in the content of surface Ni is the detachment during coke combustion of some Ni<sup>0</sup> particles located at the edges of the coke filaments (Fig. 4b), as claimed by some authors in the literature [60]. Other possibility is the migration of Ni particles from the surface to the bulk of the catalyst particle, since the high regeneration temperature promotes the formation of different Ni species interacting with the support or free.

**Table 2**



Overall, it is concluded that in order to achieve high recovery of catalytic activity for the supported catalyst after deactivation in the OSR of raw bio-oil, the *ex situ* combustion at 850 °C in air atmosphere (without gas flow and once the catalyst has been separated from the inert solid) is the best strategy. This method is able to i) remove completely the coke, ii) recover the initial NiAl<sub>2</sub>O<sub>4</sub> spinel structure of the fresh catalyst and iii) improve the dispersion of surface Ni<sup>0</sup> particles after its reduction. However, this method fails to fully re-establish the catalytic activity of the fresh catalyst due to the decrease in amount of Ni on the surface.

### 3.2. On the regenerability of the bulk catalyst

#### 3.2.1. Performance in reaction and regeneration steps

Similarly to supported catalyst, a reaction-regeneration cycle has been performed with bulk catalyst, under the conditions described in section 2.3, in order to analyze the activity recovery after the different regeneration treatments. Fig. 7 shows the evolution with time on stream of the reaction indices (bio-oil conversion and product yields) for the first reaction step (fresh catalyst) and for the second reaction step (regenerated catalysts). The bulk catalyst reaches full conversion during the first reaction together with 80 % H<sub>2</sub> yield which is higher than that obtained with the supported catalyst (Fig. 2), although the space time is lower in this case (0.045 and 0.075 g<sub>Ni</sub>h/g<sub>bio-oil</sub> for the bulk and the supported catalyst, respectively). This is explained by the higher dispersion and smaller Ni<sup>0</sup> crystallite size in the NiAl<sub>2</sub>O<sub>4</sub> catalyst after reduction (see the results in Tables 1 and 3 for fresh catalysts).

#### Figure 7

The general trend in the evolution with time on stream of reaction indices in Fig. 7 is similar to that observed in Fig. 2 for the supported catalyst. Thus, the bio-oil conversion and the yields of main products (H<sub>2</sub> and CO<sub>2</sub>) decrease (Fig. 7a, 7b and 7c, respectively), whereas the yields of CH<sub>4</sub> and light hydrocarbons do increase (Fig. 7e and 7f, respectively) and the yield of CO goes through a maximum (Fig. 7d) (because it is an intermediate product in the overall reaction scheme). Nevertheless, catalyst deactivation is considerable slower for the bulk catalyst than that for the supported catalyst. Thus, deactivation after 7 h TOS for the bulk catalyst is the same as for the supported after only 3 h TOS. The qualitative behavior of the regenerated bulk catalyst

in Fig. 7 is similar to that observed in Fig. 2 for the supported catalyst regenerated under the same conditions. In this way, the recovery of activity is hardly appreciated for the catalyst regenerated *in situ* at 650 °C (4 %, according to Eq. (5)), it is noticeable for the catalyst regenerated *in situ* at 850 °C in the fluidized bed (50 %) and it is almost complete for the sample regenerated *ex-situ* at 850 °C (97 %). This is a very interesting result, as it proves the regenerability of the bulk catalyst for the oxidative steam reforming of raw bio-oil operating under successive reaction-regeneration cycles. Furthermore, taking into account that the coke is totally removed after combustion at 650 °C (Fig. S1 of supplementary information), similarly to the supported catalyst, the different behavior of the regenerated bulk catalyst must be due to the effect the regeneration method has on the metallic properties, as shown next.

### 3.2.2. Metallic properties of the catalyst

Fig. 8 shows the TPR profiles of the bulk catalyst fresh and after regeneration at the aforementioned different conditions for coke combustion. All the samples require high temperature (850 °C) for the complete reduction of all the Ni species. The fresh catalyst has a wide and asymmetrical reduction peak between 500-850 °C, with its maximum around 770 °C, which evidences the presence of spinel type Ni species [15]. Similarly to the supported catalyst, no reduction peaks are observed for the deactivated catalyst (results not shown), which evidences that Ni<sup>0</sup> metal particles are not re-oxidized during the OSR reaction. Moreover, the TPR profiles of all samples in Fig. 8 are qualitatively similar to the corresponding supported catalyst for the same regeneration conditions (Fig. 3). Therefore, big reduction peaks are observed from 300 to 500 °C for the catalyst samples regenerated *in situ*, which correspond to the reduction of NiO species with different level of interaction with the support. The quantity of these species decreases when increasing the regeneration temperature and also their reduction requires higher temperature, thus indicating a stronger interaction with the support. The TPR profile for the catalyst regenerated *ex situ* at 850 °C is very similar to that of the fresh catalyst, with mainly NiAl<sub>2</sub>O<sub>4</sub> spinel (peak at 780 °C) and small content of NiO species.

### Figure 8

Fig. 9 shows the XRD diffractograms of the fresh, the deactivated and the regenerated bulk catalyst. Graph a corresponds to the oxidized samples (fresh and regenerated) and

graph b corresponds to the reduced samples (fresh, deactivated and regenerated). For this catalyst, the species identified in XRD diffractograms are  $\text{NiAl}_2\text{O}_4$ ,  $\text{NiO}$ ,  $\text{Al}_2\text{O}_3$  and  $\text{Ni}^0$ . The non-reduced fresh catalyst (Fig. 9a) shows only the XRD pattern of the  $\text{NiAl}_2\text{O}_4$  spinel, and after reduction (Fig. 9b) the only species observed are  $\text{Ni}^0$  and  $\text{Al}_2\text{O}_3$ , produced by the exsolution of the metal from the spinel. In the catalyst regenerated *in situ* at 650 °C the predominant specie is  $\text{NiO}$  (Fig. 9a), and the  $\text{NiAl}_2\text{O}_4$  spinel phase is almost negligible. After the regeneration *in situ* at 850 °C the initial  $\text{NiAl}_2\text{O}_4$  structure is partially recovered, although a considerably high amount of  $\text{Ni}$  is found as  $\text{NiO}$ . Finally, for the catalyst regenerated *ex situ* at 850 °C the  $\text{NiAl}_2\text{O}_4$  spinel is the prevailing species, with just little amount of  $\text{NiO}$ .

For the reduced catalyst samples (Fig. 9b), the only species are  $\text{Al}_2\text{O}_3$  and  $\text{Ni}^0$ , the latter formed from reduction of  $\text{NiO}$  and  $\text{NiAl}_2\text{O}_4$ . Nevertheless, differences in the  $\text{Ni}^0$  crystallite size are significant for the different samples (Table 3). These values have been calculated according to the Scherrer equation from the  $\text{Ni}^0$  diffraction peak in the (1 1 1) plane ( $2\theta = 44.7^\circ$ ). The  $\text{Ni}^0$  crystallite size of the fresh catalyst is 11 nm and it increases up to 20 nm after 6 h TOS, which evidences  $\text{Ni}$  sintering. After regeneration *in situ* at 650 °C, the  $\text{Ni}^0$  crystal size remains the same, but it decreases slightly (18 nm) at higher regeneration temperature (850 °C). However, when the catalyst is regenerated *ex situ* at 850 °C the crystal size is 13.5 nm, which is very similar to that of the fresh catalyst.

### Figure 9

### Table 3

$\text{Ni}$  crystal sizes for the different catalyst samples determined by the Scherrer equation (Table 3) have been confirmed by TEM analysis (Fig. 10) and the resulting PSD (Fig. 11). Thus, the fresh catalyst has a  $\text{Ni}^0$  average particle size of 10.8 nm, with quite homogeneous PSD. The average particle size of the deactivated catalyst is twice that of the fresh catalyst, and it is noteworthy that the formation of carbon filaments is not so noticeable in the bulk deactivated catalyst as in supported deactivated catalyst (Fig. 5b). The highest metal particle redispersion is attained for the catalyst regenerated *ex situ* at 850 °C. The average  $\text{Ni}^0$  particle size after this regeneration treatment is 12.6 nm, only slightly higher than that of the fresh catalyst.

**Figure 10****Figure 11**

The fresh and the regenerated samples of the bulk catalyst have been analyzed by XPS (Table 4), in order to determine the content (wt %) of the surface elements and to study the possible migration of Ni during the deactivation or regeneration steps. The surface Ni content of the catalyst after regeneration at different conditions is 75 % of that of the fresh catalyst. This proves that the loss of surface Ni in the bulk catalyst is lower than the loss in the supported catalyst (Table 2). It is noteworthy that the slightly lower amount of surface Ni in the bulk catalyst has negligible effect on its catalytic activity, and the catalyst regenerated *ex situ* at 850 °C almost recovers completely the activity of the fresh catalyst (Fig. 7).

To sum up, results described in this section prove that both an increase in temperature for coke combustion and the gas-solid contact without gas flow through the catalyst particles in an external oven favors the reassembly of the NiAl<sub>2</sub>O<sub>4</sub> spinel species in the catalyst. After the reduction of these species, Ni<sup>0</sup> crystals have high dispersion and small size, leading to the same catalytic activity as that of the fresh catalyst in the OSR of the raw bio-oil.

**4. Discussion**

Coke deposition is considered in the literature the main cause for deactivation of Ni catalysts in the reforming of oxygenates, especially when the formation of encapsulating coke (which is burnt at low temperature) is favored on the Ni active sites [51,52], which happens at low temperature, space time and S/C ratio in the reaction [21-23,32,33,52]. However, the catalytic behavior after a reaction-regeneration cycle (Figs. 2 and 7) demonstrates that encapsulating coke deposition is not the only deactivation cause. The oxidation of Ni<sup>0</sup> (the active phase for the reforming reaction) has been discarded as a possible deactivation cause, since no evidence of NiO species has been observed in the TPR profiles nor in the XRD diffractograms for neither of the deactivated catalysts. Consequently, the additional deactivation cause must be attributed to Ni<sup>0</sup> sintering, which contributes to the decrease in the activity with TOS. This hypothesis has been proved by means of XRD diffractograms, which have narrower Ni<sup>0</sup> diffraction peaks for the deactivated catalysts, thus evidencing bigger Ni<sup>0</sup> crystallite size, and also by TEM

images, which show a significant increase in the average metal particle size for the deactivated catalysts (Tables 1 and 3).

Sintering of the metallic function is generally irreversible in catalysis. In order to avoid it, the development of redispersion methods are of paramount importance. Due to its economic viability, the redispersion of Pt and Pt/Al<sub>2</sub>O<sub>3</sub> catalysts, such as those employed in the reforming of hydrocarbons, have received increasing attention [61-64]. However, metal redispersion has been scarcely studied for Ni catalysts used in reforming reactions. Recently, Yang [14] proved by TEM analysis that, after a steam treatment of a Ni catalyst deactivated at 700 °C in the steam reforming of CH<sub>4</sub>, not only was the sulfur eliminated but also the Ni<sup>0</sup> particles recovered the initial size in the fresh catalyst. In our study, we have explored the metal redispersion during the same regeneration step by coke combustion, required due to the rapid coke deposition in the OSR of bio-oil (although the deposition rate is lower than that of the non-oxidative SR). The results of Ni<sup>0</sup> crystallite size (Table 1 and Fig. 5 for supported catalyst, and Table 3 and Fig. 10 for bulk catalyst) prove that Ni redispersion is possible for both Ni based catalysts, provided that suitable operating conditions are used in the regeneration step by coke combustion. Furthermore, by comparing the Ni<sup>0</sup> particle size of the regenerated catalysts with their corresponding kinetic behavior (Fig. 2 and 7 for supported and bulk catalysts, respectively), it is concluded that the recovery of activity is directly related to the Ni<sup>0</sup> particle size of the regenerated catalysts. Results shown in section 3 have highlighted as well the importance of the combustion conditions and the catalyst structure in order to recover the Ni<sup>0</sup> particle size and thus, the activity of the fresh catalyst.

The comparison of both NiAl<sub>2</sub>O<sub>4</sub> based catalysts highlights the importance of the synthesis method of the spinel precursor (supported or bulk catalyst) for their regenerability and also the importance of the regeneration conditions for the reassembly of the NiAl<sub>2</sub>O<sub>4</sub> spinel phase, which is key for the redispersion of the Ni<sup>0</sup> active sites after the reduction. On the contrary, large metal particles are formed when NiO is the prevailing Ni specie in the regenerated catalyst. These conclusions were obtained by comparing the average metal particle size with its corresponding TPR profile (Fig. 3 and 8, corresponding to supported and bulk catalysts, respectively) which allows to

relate the Ni<sup>0</sup> particle size with the presence of the different Ni oxidized species (NiO or NiAl<sub>2</sub>O<sub>4</sub>) in the regenerated catalysts.

The temperature and the gas-solid contact in the regeneration step by coke combustion have a significant effect in the formation of different oxidized Ni species (NiO and NiAl<sub>2</sub>O<sub>4</sub>). TPR and XRD analysis of the regenerated catalysts (Fig. 3 and 4a for supported catalyst and Figs. 8 and 9a for bulk catalyst) prove the smaller quantity of the NiAl<sub>2</sub>O<sub>4</sub> specie for both catalysts after coke combustion *in situ* at 650 °C in the fluidized bed, the NiO species being prevalent. Temperature increase up to 850 °C boosts the formation of the spinel and this effect is more accentuated when the combustion takes place *ex situ* in the external oven. A possible explanation could be that the conditions employed in the *ex-situ* combustion (in air atmosphere with no gas flow and after removing the inert solid (SiC) employed in the reaction) favor the solid-solid contact for the synthesis reaction of the spinel ( $\text{NiO} + \text{Al}_2\text{O}_3 \rightarrow \text{NiAl}_2\text{O}_4$ ), and promote the creation of 'hot spots' during the combustion of coke. In fact, some authors have demonstrated the convenience of exceeding 850 °C in the preparation of Ni/Al<sub>2</sub>O<sub>3</sub> catalysts with the purpose of obtaining only the NiAl<sub>2</sub>O<sub>4</sub> spinel structure [65,66].

The comparison of the regeneration efficiency for both catalysts under the most favorable regeneration conditions, demonstrates the relevance of the structure of the fresh catalyst in its regenerability. Under these regeneration conditions, the activity recovery of the bulk catalyst is complete but partial for supported catalyst, although for the latter the Ni<sup>0</sup> crystal size is even smaller than that of the fresh catalyst. This difference in the regenerability of the catalysts is likely due to differences in the evolution of Ni in the cycles of formation and combustion of coke. Thus, the supported catalyst loses Ni (mainly from the surface) after the coke combustion (Table 2). One of the possible causes is the detachment of the Ni-particles from the support when the C-filaments are being formed (observed by TEM, Fig. 5), which has been also observed by other authors [27,60]. Other possible explanation is the migration of Ni towards the bulk of the catalyst, during coke combustion. These phenomena, and thus the consequent decrease in Ni on the surface of the catalyst, are less accentuated for the bulk catalyst, which recovers completely its initial activity after the *ex situ* combustion of the coke at 850 °C, without any additional heat treatment.

## 5. Conclusions

The causes of deactivation in the OSR of raw bio-oil at 700 °C for the supported Ni/La<sub>2</sub>O<sub>3</sub>- $\alpha$ -Al<sub>2</sub>O<sub>3</sub> and the bulk NiAl<sub>2</sub>O<sub>4</sub> catalysts, both in the form of Ni-Al spinel phase, are coke deposition and Ni sintering. Consequently, for the recovery of the initial activity of the fresh catalyst, a regeneration treatment is needed which not only removes completely the formed coke, but also restores the original NiAl<sub>2</sub>O<sub>4</sub> structure, thus favoring the redispersion of the Ni<sup>0</sup> sites after reduction. Therefore, besides a proper catalyst design, with a homogeneous distribution of the NiAl<sub>2</sub>O<sub>4</sub> spinel, the viability of this process requires the proposal of adequate regeneration conditions.

For both catalysts, coke combustion at high temperature (850 °C) enhances the contact between NiO and Al<sub>2</sub>O<sub>3</sub> (without inert and/or catalyst motion) and leads to their reassembly to form NiAl<sub>2</sub>O<sub>4</sub> spinel phase in the regenerated catalyst, which after reduction results in small and well dispersed Ni<sup>0</sup> particles. The redispersion in the regenerated bulk catalyst generates Ni<sup>0</sup> particles with the same size as those in the fresh catalyst. For the supported catalyst, the particles formed after regeneration and subsequent to reduction are even smaller than those in the fresh catalyst.

The different activity recovery of the catalysts is explained by the different capability to retain the Ni surface species throughout a reaction-regeneration cycle. Accordingly, the decrease in Ni for the bulk catalyst after the combustion is very low, whereas for the supported catalyst, the loss of Ni (mainly on the surface) is high. However, the activity loss is of around 15 % due to the smaller size of Ni<sup>0</sup> particles after regeneration. Therefore, the bulk catalyst is suitable for use in the reforming of raw bio-oil in reaction-regeneration cycles, since its activity can be fully recovered provided that the regeneration conditions are suitable for achieving both total coke removal and Ni redispersion. This result is encouraging for future industrial implantation of bio-oil reforming using economically viable catalysts based on NiAl<sub>2</sub>O<sub>4</sub> spinel.

## Acknowledgements

This work was carried out with the financial support of the Department of Education Universities and Investigation of the Basque Government (IT748-13), the Ministry of Economy and Competitiveness of the Spanish Government jointly with the European

Regional Development Funds (AEI/FEDER, UE) (Proyectos CTQ2012-35263 and CTQ2015-68883-R and Ph.D. grant BES-2013-063639 for A. Arandia).



## References

- [1] M. Ball, M. Weeda, The hydrogen economy – Vision or reality? *Int. J. Hydrogen Energy* 40 (2015) 7903–7919.
- [2] R. Moliner, M.J. Lázaro, I. Suelves, Analysis of the strategies for bridging the gap towards the Hydrogen energy, *Int. J. Hydrogen Energy* 41 (2016) 19500–19508.
- [3] P. Mohanty, K.K. Pant, R. Mittal, Hydrogen generation from biomass materials: challenges and opportunities, in *advances in bioenergy: The sustainability challenge*, (eds P. D. Lund, J. Byrne, G. Berndes and I. A. Vasalos), John Wiley & Sons, Ltd, Oxford, 2016.
- [4] D. Li, X. Li, J. Gong, Catalytic reforming of oxygenates: State of the art and future prospects, *Chem. Rev.* 116 (2016) 11529–11613.
- [5] P. Lanzafame, G. Centi, S. Perathoner, Evolving scenarios for biorefineries and the impact on catalysis, *Catal. Today* 234 (2014) 2–12.
- [6] D. Meier, B. van de Beld, A.V. Bridgwater, D.C. Elliott, A. Oasmaa, F. Preto, State-of-the-art of fast pyrolysis in IEA bioenergy member countries, *Renew. Sust. Energy Rev.* 20 (2013) 619–641.
- [7] D. Carpenter, T.L. Westover, S. Czernik, W. Jablonski, Biomass feedstocks for renewable fuel production: A review of the impacts of feedstock and pretreatment on the yield and product distribution of fast pyrolysis bio-oils and vapors, *Green Chem.* 16 (2014) 384–406.
- [8] S. Czernik, R. French, Distributed production of hydrogen by auto-thermal reforming of fast pyrolysis bio-oil, *Int. J. Hydrogen Energy* 39 (2014) 744–750.
- [9] G. Chen, J. Tao, C. Liu, B. Yan, W. Li, X. Li, Hydrogen production via acetic acid steam reforming: A critical review on catalysts, *Renew. Sust. Energ. Rev.* 79 (2017) 1091–1098.
- [10] J. Sehested, J.A.P. Gelten, S. Helveg, Sintering of nickel catalysts: Effects of time, atmosphere, temperature, nickel-carrier interactions, and dopants, *Appl. Catal. A* 309 (2006) 237–246.
- [11] M. Ashrafi, C. Pfeifer, T. Pröll, H. Hofbauer, Experimental study of model biogas catalytic steam reforming: 2. Impact of sulfur on the deactivation and regeneration of Ni-based catalysts, *Energy Fuels* 22 (2008) 4190–4195.
- [12] S.M. Hashemnejad, M. Parvari, Deactivation and regeneration of nickel-based catalysts for steam-methane reforming, *Chin. J. Catal.* 32 (2011) 273–279.
- [13] S. Appari, V.M. Janardhanan, R. Bauri, S. Jayanti, Deactivation and regeneration of Ni catalyst during steam reforming of model biogas: An experimental investigation, *Int. J. Hydrogen Energy* 39 (2014) 297–304.
- [14] X. Yang, An experimental investigation on the deactivation and regeneration of a steam reforming catalyst, *Renew. Energy* 112 (2017) 17–24.
- [15] C. Montero, A. Remiro, A. Arandia, P.L. Benito, J. Bilbao, A.G. Gayubo, Reproducible performance of a Ni/La<sub>2</sub>O<sub>3</sub>- $\alpha$ -Al<sub>2</sub>O<sub>3</sub> catalyst in ethanol steam

- reforming under reaction-regeneration cycles, *Fuel Process. Technol.* 152 (2016), 215–222.
- [16] Y.C. Sharma, A. Kumar, R. Prasad, S.N. Upadhyay, Ethanol steam reforming for hydrogen production: Latest and effective catalyst modification strategies to minimize carbonaceous deactivation, *Renew. Sust. Energ. Rev.* 74 (2017) 89–103.
- [17] E.A. Sanchez, R.A. Comelli, Hydrogen by glycerol steam reforming on a nickel-alumina catalyst: Deactivation processes and regeneration, *Int. J. Hydrogen Energy* 37 (2012) 14740–14746.
- [18] D.F.P. Suffredini, V.V. Thyssen, P.M.M. de Almeida, R.S. Gomes, M.C. Borges, A.M. Duarte de Farias, E.M. Assaf, M. A. Fraga, S.T. Brandao, Renewable hydrogen from glycerol reforming over nickel aluminate-based catalysts, *Catal. Today* 289 (2017) 96–104.
- [19] L. An, C. Song, Y. Yang, J. Zhang, L. He, The influence of Ni loading on coke formation in steam reforming of acetic acid. *Renew. Energy*, 36 (2011) 930-935.
- [20] G. Garbarino, A. Lagazzo, P. Riani, G. Busca, Steam reforming of ethanol-phenol mixture on Ni/Al<sub>2</sub>O<sub>3</sub>: Effect of Ni loading and Sulphur deactivation. *Appl. Catal. B* 129 (2013) 460–472.
- [21] A. Remiro, B. Valle, A.T. Aguayo, J. Bilbao, A.G. Gayubo, Operating conditions for attenuating Ni/La<sub>2</sub>O<sub>3</sub>– $\alpha$ -Al<sub>2</sub>O<sub>3</sub> catalyst deactivation in the steam reforming of bio-oil aqueous fraction, *Fuel Process. Technol.* 115 (2013) 222–232.
- [22] A. Ochoa, B. Aramburu, B. Valle, D.E. Resasco, J. Bilbao, A.G. Gayubo, P. Castaño, Role of oxygenates and effect of operating conditions in the deactivation of a Ni supported catalyst during the steam reforming of bio-oil, *Green Chem.* 19 (2017) 4315–4333.
- [23] A. Remiro, A. Arandia, J. Bilbao, A.G. Gayubo, Comparison of Ni based and Rh based catalyst performance in the oxidative steam reforming of raw bio-oil, *Energy Fuels* 31 (2017) 7147–7156.
- [24] A. Simson, R. Farrauto, M. Castaldi, Steam reforming of ethanol/gasoline mixtures: Deactivation, regeneration and performance, *Appl. Catal. B* 106 (2011) 295–303.
- [25] L. Bednarczuk, P. Ramirez de la Piscina, N. Homs, Efficient CO<sub>2</sub>-regeneration of Ni/Y<sub>2</sub>O<sub>3</sub>-La<sub>2</sub>O<sub>3</sub>-ZrO<sub>2</sub> systems used in the ethanol steam reforming for hydrogen production, *Int. J. Hydrogen Energy* 41 (2016) 19509–19517.
- [26] B. Rego de Vasconcelos, D.P. Minh, P. Sharrock, A. Nzihou, Regeneration study of Ni/hydroxyapatite spent catalyst from dry reforming, *Catal. Today* (2017) <http://dx.doi.org/10.1016/j.cattod.2017.05.092>.
- [27] C. Wu, R. Liu, Sustainable hydrogen production from steam reforming of bio-oil model compound based on carbon deposition/elimination, *Int. J. Hydrogen Energy* 36 (2011) 2860–2868.
- [28] B. Valle, B. Aramburu, A. Remiro, J. Bilbao, A.G. Gayubo, Effect of calcination/reduction conditions of Ni/La<sub>2</sub>O<sub>3</sub>– $\alpha$ -Al<sub>2</sub>O<sub>3</sub> catalyst on its activity and stability for hydrogen production by steam reforming of raw bio-oil/ethanol, *Appl. Catal. B* 147 (2014) 402–410.

- [29] N. Salhi, A. Boulahouache, C. Petit, A. Kiennemann, C. Rabia, Steam reforming of methane to syngas over  $\text{NiAl}_2\text{O}_4$  spinel catalysts, *Int. J. Hydrogen Energy* 36 (2011) 11433–11439.
- [30] A. Remiro, B. Valle, B. Aramburu, A.T. Aguayo, J. Bilbao, A.G. Gayubo, Steam reforming of the bio-oil aqueous fraction in a fluidized bed reactor with in-situ  $\text{CO}_2$  capture, *Ind. Eng. Chem. Res* 52 (2013) 17087–17098.
- [31] A. Remiro, B. Valle, A.T. Aguayo, J. Bilbao, A.G. Gayubo, Steam reforming of raw bio-oil in a fluidized bed reactor with prior separation of pyrolytic lignin. *Energy Fuels* 27 (2013) 7549–7559.
- [32] B. Valle, B. Aramburu, M. Olazar, J. Bilbao, A.G. Gayubo, Steam reforming of raw bio-oil over  $\text{Ni/La}_2\text{O}_3\text{-Al}_2\text{O}_3$ : Influence of temperature on product yields and catalyst deactivation, *Fuel* 216 (2018), 463–474.
- [33] B. Valle, B. Aramburu, P.L. Benito, J. Bilbao, A.G. Gayubo, Biomass to hydrogen-rich gas via steam reforming of raw bio-oil over  $\text{Ni/La}_2\text{O}_3\text{-Al}_2\text{O}_3$  catalyst: Effect of space-time and steam-to-carbon ratio, *Fuel* 216 (2018) 445–455.
- [34] J. Vicente, C. Montero, J. Ereña, M.J. Azkoiti, J. Bilbao, A.G. Gayubo, Coke deactivation of Ni and Co catalysts in ethanol steam reforming at mild temperatures in a fluidized bed reactor, *Int. J. Hydrogen Energy* 39 (2014) 12586–12596.
- [35] A. Remiro, B. Valle, L. Oar-Arteta, A.T. Aguayo, J. Bilbao, A.G. Gayubo, Hydrogen production by steam reforming of bio-oil/bio-ethanol mixtures in a continuous thermal-catalytic process, *Int. J. Hydrogen Energy* 39 (2014) 6889–6898.
- [36] B. Valle, A. Remiro, A.T. Aguayo, J. Bilbao, A.G. Gayubo, Catalysts of  $\text{Ni}/\alpha\text{-Al}_2\text{O}_3$  and  $\text{Ni/La}_2\text{O}_3\text{-}\alpha\text{Al}_2\text{O}_3$  for hydrogen production by steam reforming of bio-oil aqueous fraction with pyrolytic lignin retention, *Int. J. Hydrogen Energy* 38 (2013) 1307–1318.
- [37] L. Garcia, R. French, S. Czernik, E. Chornet, Catalytic steam reforming of bio-oils for the production of hydrogen: Effects of catalyst composition. *Appl. Catal. A* 201 (2000) 225–239.
- [38] M.B.I. Chowdhury, M.M. Hossain, P.A. Charpentier, Effect of supercritical water gasification treatment on  $\text{Ni/La}_2\text{O}_3\text{-Al}_2\text{O}_3$ -based catalysts. *Appl. Catal. A* 405 (2011) 84–92.
- [39] A.N. Fatsikostas, D.I. Kondarides, X.E. Verykios, Production of hydrogen for fuel cells by reformation of biomass-derived ethanol. *Catal. Today* 75 (2002) 145–155.
- [40] M.M. Yung, W.S. Jablonski, K.A. Magrini-Bair, Review of catalytic conditioning of biomass-derived syngas. *Energy Fuels* 23 (2009) 1874–1887.
- [41] A. Serrano-Lotina, L. Rodríguez, G. Muñoz, A.J. Martín, M.A. Folgado, L. Daza, Biogas reforming over  $\text{La-NiMgAl}$  catalysts derived from hydrotalcite-like structure: Influence of calcination temperature, *Catal. Commun.* 12 (2011) 961–967.
- [42] A. Al-Ubaid, E.E. Wolf, Steam reforming of methane on reduced non-stoichiometric nickel aluminate catalysts, *Appl. Catal.* 40 (1988) 73–85.

- [43] L. García, M.L. Salvador, J. Arauzo, R. Bilbao, CO<sub>2</sub> as a gasifying agent for gas production from pine sawdust at low temperatures using a Ni/Al coprecipitated catalyst, *Fuel Process. Technol.* 69 (2001) 157–174
- [44] A.R. Fernández-Akarregi, J. Makibar, G. López, M. Amutio, M. Olazar, Design and operation of a conical spouted bed reactor pilot plant (25 kg/h) for biomass fast pyrolysis, *Fuel Process. Technol.* 112 (2013) 48–56.
- [45] S.A. Channiwala, P.P. Parikh, A unified correlation for estimating HHV of solid, liquid and gaseous fuels. *Fuel* 81 (2002) 1051–1063.
- [46] R. Palos, A. Gutiérrez, J.M. Arandes, J. Bilbao, Catalyst used in fluid catalytic cracking (FCC) unit as a support of NiMoP catalyst for light cycle oil hydroprocessing, *Fuel* 216 (2018) 142–152.
- [47] D.C. Elliot, T.R. Hart, G.G. Neuenschwander, L.J. Rotness, M.V. Olarte, A.H. Zacher, Y. Solantausta, Catalytic hydroprocessing of fast pyrolysis bio-oil from pine sawdust, *Energy Fuels* 26 (2012) 3891–3896.
- [48] M. Patel, A. Kumar, Production of renewable diesel through the hydroprocessing of lignocellulosic biomass-derived bio-oil: A review, *Renew. Sust. Ener. Rev.* 58 (2016) 1293–1307.
- [49] B. Valle, A. Remiro, B. Aramburu, J. Bilbao, A.G. Gayubo, Strategies for maximizing the bio-oil valorization by catalytic transformation, *J. Cleaner Prod.* 88 (2015) 345–348.
- [50] A. Arandia, A. Remiro, B. Valle, J. Bilbao, A.G. Gayubo, Operating strategies for the oxidative steam reforming (OSR) of raw bio-oil in a continuous two-step system, *Chem. Eng. Trans.* 57 (2017) 217–222.
- [51] C. Montero, A. Ochoa, P. Castaño, J. Bilbao, A.G. Gayubo, Monitoring Ni<sup>0</sup> and coke evolution during the deactivation of a Ni/La<sub>2</sub>O<sub>3</sub>- $\alpha$ -Al<sub>2</sub>O<sub>3</sub> catalyst in ethanol steam reforming in a fluidized bed, *J. Catal.* 331 (2015) 181–192.
- [52] J. Vicente, J. Ereña, C. Montero, M. J. Azkoiti, J. Bilbao, A.G. Gayubo, Reaction pathway for ethanol steam reforming on a Ni/SiO<sub>2</sub> catalyst including coke formation, *Int. J. Hydrogen Energy* 39 (2014) 18820–18834.
- [53] A. Arandia, A. Remiro, J. Bilbao, A.G. Gayubo, Reaction conditions effect and pathways in the oxidative steam reforming of raw bio-oil on a Rh/CeO<sub>2</sub>-ZrO<sub>2</sub> catalyst in a fluidized bed reactor, *Int. J. Hydrogen Energy* 42 (2017) 29175–29185.
- [54] A.G. Gayubo, B. Valle, B. Aramburu, C. Montero, J. Bilbao, Kinetic model considering catalyst deactivation for the steam reforming of bio-oil over Ni/La<sub>2</sub>O<sub>3</sub>- $\alpha$ -Al<sub>2</sub>O<sub>3</sub> catalyst, *Chem. Eng. J.* 332 (2018) 192–204.
- [55] C. Li, Y. Chen, Temperature-programmed-reduction studies of nickel oxide/alumina catalysts: effects of the preparation method, *Thermochim. Acta* 256 (1995) 457–465.
- [56] S. Natesakhawat, O. Oktar, U.S. Ozkan, Effect of lanthanide promotion on catalytic performance of sol-gel Ni/Al<sub>2</sub>O<sub>3</sub> catalysts in steam reforming of propane, *J. Mol. Catal. A Chem.* 241 (2005) 133–146.

- [57] A.M. Karim, Y. Su, J. Sun, C. Yang, J.J. Strohm, D.L. King, Y. Wang, A comparative study between Co and Rh for steam reforming of ethanol, *Appl. Catal. B* 96 (2010) 441–448.
- [58] S. Helveg, J. Sehested, J.R. Rostrup-Nielsen, Whisker carbon in perspective, *Catal. Today* 178 (2011) 42–46.
- [59] Y. Jiao, J. Zhang, Y. Du, F. Li, C. Li, J. Lu, J. Wang, Y. Chen, Hydrogen production by catalytic steam reforming of hydrocarbon fuels over Ni/Ce-Al<sub>2</sub>O<sub>3</sub> bifunctional catalysts: Effects of SrO addition, *Int. J. Hydrogen Energy* 41 (2016) 13436–13447.
- [60] I. Czekaj, F. Loviat, F. Raimondi, J. Wambach, S. Biollaz, A. Wokaun, Characterization of surface processes at the Ni-based catalyst during the methanation of biomass-derived synthesis gas: X-ray photoelectron spectroscopy (XPS), *Appl. Catal. A* 329 (2007) 68–78.
- [61] B. Didillon, Catalyst regeneration process and use of the catalyst in hydrocarbon conversion processes, U.S. Patent 5,672,801, 30 September 1997.
- [62] C.L. Pieck, C.R. Vera, J.M. Parera, Study of industrial and laboratory regeneration of Pt-Re/Al<sub>2</sub>O<sub>3</sub> catalysts, *Stud. Surf. Sci. Catal.* 139 (2001) 279–286.
- [63] A. Monzon, T.F. Garetto, A. Borgna, Sintering and redispersion of Pt/ $\gamma$ -Al<sub>2</sub>O<sub>3</sub> catalysts: a kinetic model, *Appl. Catal. A* 248 (2003) 279–289.
- [64] M.D. Argyle, C.H. Bartholomew, Heterogeneous catalyst deactivation and regeneration: a review, *Catalysts* 5 (2015) 145–269.
- [65] L. Zhou, L. Li, N. Wei, J. Li, J.M. Basset, Effect of NiAl<sub>2</sub>O<sub>4</sub> formation on Ni/Al<sub>2</sub>O<sub>3</sub> stability during dry reforming of methane, *ChemCatChem* 7 (2015) 2508–2516.
- [66] Z. Wang, X. Hu, D. Dong, G. Parkinson, C.Z. Li, Effects of calcination temperature of electrospun fibrous Ni/Al<sub>2</sub>O<sub>3</sub> catalysts on the dry reforming of methane, *Fuel Process. Technol.* 155 (2017) 246–251.

## Figure Captions

- Figure 1.** States of the catalyst in a reaction-regeneration cycle.
- Figure 2.** Evolution with TOS of conversion (a) and yield of H<sub>2</sub> (b), CO<sub>2</sub> (c) CO (d), CH<sub>4</sub> (e), and hydrocarbons (f) in the OSR of bio-oil over the supported catalyst, fresh and after different regeneration conditions. Reaction conditions: 700 °C; space time, 0.75 g<sub>catalyst</sub>h/g<sub>bio-oil</sub>; S/C, 6; O/C, 0.34. Regeneration conditions: coke combustion in air, *in situ* at 650 and 850 °C, and *ex situ* in an oven at 850 °C; time, 4h.
- Figure 3.** TPR profiles of the supported catalyst, fresh and under different regeneration conditions.
- Figure 4** XRD diffractograms of the supported catalyst, fresh and after different regeneration conditions. Graph a: samples before reduction. Graph b: samples after reduction.
- Figure 5.** TEM images of supported catalyst, fresh (a), deactivated (b), regenerated *ex situ* at 850 °C (c), regenerated *in situ* at 850 °C (d), and regenerated *in situ* at 650 °C (e).
- Figure 6.** Particle size distribution of the supported catalyst, fresh, deactivated and after different regeneration conditions.
- Figure 7.** Evolution with TOS of conversion (a) and yield of H<sub>2</sub> (b), CO<sub>2</sub> (c) CO (d), CH<sub>4</sub> (e), and hydrocarbons (f) in the OSR of bio-oil over the bulk, catalyst, fresh and after different regeneration conditions. Reaction conditions: 700 °C; space time, 0.15 g<sub>catalyst</sub>h/g<sub>bio-oil</sub>; S/C, 6; O/C, 0.34. Regeneration conditions: coke combustion in air, *in situ* a 650 and 850 °C, and *ex situ* in an oven at 850 °C; time, 4h.
- Figure 8.** TPR profiles of the bulk catalyst, fresh and after different regeneration conditions.
- Figure 9.** XRD diffractograms of the bulk catalyst, fresh and after different regeneration conditions. Graph a: samples before reduction. Graph b: samples after reduction.

**Figure 10.** TEM images of the bulk catalyst, fresh (a), deactivated (b), regenerated *ex situ* at 850 °C (c), regenerated *in situ* at 850 °C (d), and regenerated *in situ* at 650 °C (e).

**Figure 11.** Particle size distribution of the bulk catalyst, fresh, deactivated and after different regeneration conditions.

### Supplementary information

**Figure S1.** TPO profiles for the supported and bulk catalysts deactivated after 3 h and 7 h, respectively, under the following reaction conditions: 700 °C; space time,  $0.75 \text{ g}_{\text{catalyst}}\text{h}/\text{g}_{\text{bio-oil}}$  (supported catalyst) and  $0.15 \text{ g}_{\text{catalyst}}\text{h}/\text{g}_{\text{bio-oil}}$  (bulk catalyst); S/C, 6; O/C, 0.34.

**Figure S2.** Evolution with TOS of conversion (circle) and yield of H<sub>2</sub> (triangle) in the OSR of bio-oil over the supported catalyst after different *in situ* regeneration treatments: coke combustion at 650 °C (full dots); coke combustion at 650 °C followed by steaming at 800 °C (empty dots). Reaction conditions: 700 °C; space time,  $0.75 \text{ g}_{\text{catalyst}}\text{h}/\text{g}_{\text{bio-oil}}$ ; S/C, 6; O/C, 0.34.